PROCEEDINGS OF THE INTERNATIONAL CONFERENCE NANOMATERIALS: APPLICATIONS AND PROPERTIES
Vol. **1** No 4, 04MFPN12(6pp) (2012)

Quantum Nanomagnetism

J. Tejada*, S. Vélez, R. Zarzuela

University of Barcelona, Diagonal 647, 08028 Barcelona, Spain

(Received 03 July 2012; published online 07 August 2012)

In this paper we discuss some of our most important results in quantum nanomagnets in the last twenty years. We start with the tunnelling of the magnetic moment in single domain particles, then we will move to molecular magnets to explain both resonant spin tunnelling and quantum magnetic deflagration and we will finish discussing the quantum phenomena recently observed in vortices of two dimensional disks and in type I superconductors. Probably the most important question to answer in the cases presented in this paper refers to the possibility to detect both coherent phonons and photons from the demagnetization process of molecular magnets as well as the fact to go deeper in the quantum phenomena observed in vortices of two dimensional disks and in type I superconductors.

Keywords: Macroscopic quantum tunneling, Molecular magnets, Magnetic vortices, Type-I superconductivity.

PACS numbers: 75.45.+j, 75.70.Kw, 74.25.Ha

1. SINGLE DOMAIN PARTICLES

Magnetism of solids can be studied at three different length scales, the nanoscale which corresponds to the magnetic phenomena taking place at the atomic and molecular level, the mesoscopic scale characterized by spin Hamiltonians trying to explain, for example, the existence of a constant local spin density and the macroscopic scale in which it is explained the existence of magnetic domains and domain walls, spin waves and magnetic resonance and where the motion of the magnetization is explained by the very fundamental law described by the Landau-Lifshitz equation.

The exchange interaction between two atomic spins can be modelled by $-\mathrm{J}(r)\ \mathbf{s}_1\cdot\mathbf{s}_2$ where r is the distance between the two atoms and J is called the exchange constant. In the case of having N atoms the spin Hamiltonian is

$$H_{ex} = -\sum_{i<j} J(r_{ij})\mathbf{s}_i \cdot \mathbf{s}_j \,, \qquad (1)$$

where $\mathbf{s}_i$ is the spin of the i-th atom, $r_{ij} = r_{ji}$ is the distance between the atoms i and j. The Hamiltonian of equation (1) commutes with each component of the total spin $\mathbf{S} = \Sigma\mathbf{s}_i$. Associated to this total spin we may also write a total magnetic moment **M** which still satisfies the quantum commutation relation

$$M_i M_j - M_j M_i = 2i\mu_B \varepsilon_{ijk} M_k \,, \qquad (2)$$

It is clear that as soon as $|\mathbf{M}|$ significantly exceeds the value of μ_B (Bohr magneton) the right hand of equation (2) becomes small compared with each of the two terms on the left hand side of that equation. That is, for values of $|\mathbf{M}|$ greater than thousand Bohr magnetons the magnetic moment $|\mathbf{M}|$ can be assumed to behave classically while for the case of $|\mathbf{M}|$ of few tens μ_B the commutation relation remains valid and the magnetic moment **M** can be considered to obey the laws of Quantum Mechanics.

To start with, we will discuss the physics of the nanomagnets called single domain particles. The fact that equation (1) is invariant under simultaneous rotation of all spins makes that the magnetic energy does not depend on the orientation of the total spin **S**. But it is well known that all magnets have the so called easy and hard directions as a consequence of the existence of the magnetic anisotropy, which is of relativistic origin as it is associated to the spin-orbit coupling. In the majority of the cases the exchange energy is order of magnitude larger than the anisotropy energy and from now we will consider that our nanomagnets have a total spin **S**.

A property of small ferro- or ferromagnetic particles is that below a certain size they do not split into magnetic domains, i.e., such a particle is a uniformly magnetized single domain. Mesoscopic particles of magnetic metals and oxides are single domain: they are small magnets with a certain location of the north and south poles. In the absence of the external magnetic field, the energy of a single domain particle does not change if its magnetic poles are interchanged. Consequently there is the same probability of finding the particle in either state [1]. In the two states the energy of the particle is minimal and are separated by an anisotropy energy barrier U, on a linear scale with the volume of the particle. To take the magnetic moment from the easy direction cost energy and this can be done by applying the external magnetic field at a certain angle to the easy axis direction. The magnetic poles return to their original positions after the external magnetic field is switched off. This give rise to the so called time dependent phenomena or magnetic relaxation. The key idea of magnetic relaxation is that, as one applies a magnetic field to a magnetic system, the magnetic moment of a such system has a two-step evolution. The first, the rapid step finishes when the system reaches the critical state; and the second

* jtejada@ubxlab.com

stage, the slow evolution, which is experimentally detected, occurs in the presence of barriers.

Real mesoscopic systems contain volumes and have an exponential large distribution of relaxation times. This explains why the magnetic relaxation of these systems obeys the logarithmic law below the so called blocking temperature [2], which corresponds to the temperature at which the relaxation time of the magnetic moment of the particles coincides with the experimental resolution time:

$$M(t) = M(t_0)[1 - S\ln(t/\tau)], \quad (3)$$

being S the magnetic viscosity, t_0 the initial time when the relaxation starts and τ the so called attempt time which is of the order of the inverse of the ferromagnetic resonance frequency.

In 1988, it was predicted by Chudnovsky and Gunther [3] that at low temperature the magnetic moment could tunnel quantum mechanically through the barrier U with a probability of the order of exp(-B) which is independent of temperature. One can define a crossover temperature T_c below which quantum underbarrier transitions dominate, $k_B T_c = U/B$. In the classical regime S should depend on T while in the case of tunnelling of the magnetic moment S should be independent of temperature. In Figure 1 we show the case of the magnetic relaxation of Fe_3Tb for different magnetic fields [4]. From this figure it is clearly stated that $S(T)$ decreases with temperature from the so called blocking temperature, $T_b = U/k_B\ln(t/\tau)$ (we only show the very low temperature regime) until it reaches the lowest temperature interval at which S is constant. The values of both $S(T)$ and T_c depend on the magnitude of the applied field during the relaxation [4].

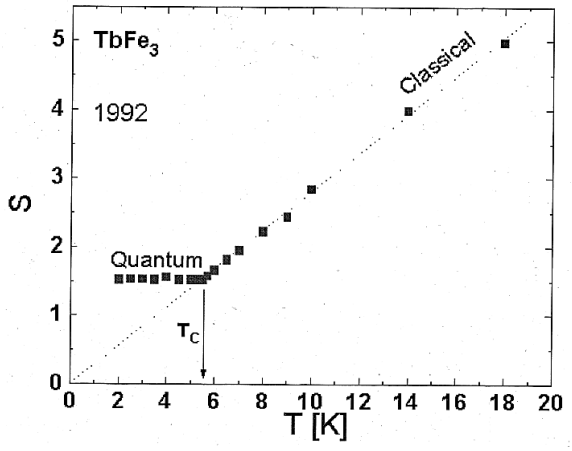

Fig. 1 – The low temperature dependence of the magnetic viscosity for $TbFe_3$

2. MOLECULAR MAGNETS

Molecular magnets are rather simple systems, which facilitates their theoretical consideration and interpretation of experiments. The current great interest of physics in these systems was ignited by the discovery of the quantum stepwise magnetization curve in the Mn_{12}-acetate [5]. In most of the cases molecular magnets can be described by a relative simple spin Hamiltonian, for example:

$$\hat{H} = -D\hat{S}_z^2 - g\mu_B\hat{S}_z H_z - g\mu_B\hat{S}_x H_x . \quad (3)$$

In the case of the molecular magnet denoted by Mn_{12}-acetate, the total spin is $S = 10$ and the system is, therefore, described by $2S + 1$ energy levels, which in the absence of the transverse field H_x are labelled by the spin projection m on the z-axis and their energy eigenvalues are given by $\varepsilon_m = -D\,m^2 - g\,\mu_B\,\mathrm{m}\,H_z$. It can be easily checked that for regularly spaced values of the longitudinal field H_z satisfying $g\,\mu_B\,H_z = k\,D$, where $k = \{0, \pm1, \pm2 \ldots\}$, the energy levels on both sides of the barrier (ε_m, $\varepsilon_{m'}$) are pair-wise degenerate, $m < 0$ and $m' = -m - k$.

Supposing we have a molecular cluster with the spin Hamiltonian described by equation (4) and the z component of the magnetic field changes from a large negative to a large positive value. At the field values corresponding to resonances between levels at the two sides of the barrier height the molecules of the nanomagnet can tunnel from the level $m = -S$ to the $m' = S - \mathrm{k}$. It will then decay down to the ground state at this side of the barrier height which is the level $m = S$. This decay process will be followed by the emission of either photons or phonons. The important points to consider, therefore, are that as the field is swept from the negative to the positive values we will observe jumps in the magnetization curve at the resonant fields and these molecules can be used as sources of phonons or/and photons. The spin tunneling probability depends very much on the value of the levels m and m': in fact, it has a much higher probability to occur across the barrier from an excited state than from $m = -S$. Thus the jumps observed in the quantum magnetization curve will also depend on temperature. This allows to observe in macroscopic experiments quantum effects such as thermally resonant spin tunnelling [6, 7], see Figure 2, spin Berry's phase [8] and quantum selection rules for the absorption of electromagnetic radiation [9-11].

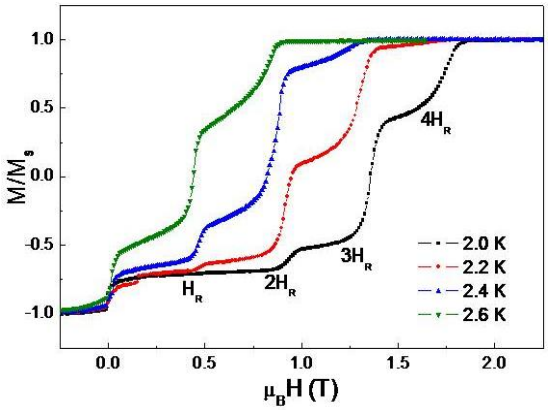

Fig. 2 – Hysteresis loops of a Mn_{12}-acetate crystal in a field parallel to the anisotropy axis

The decay process of the spin levels of the molecular magnets is mainly mediated by phonons as the phonon density is much higher than the photon density. In order to have the emission of electromagnetic radiation, the number of molecules cooperating coherently should be at least as high as the ratio between

the transition probability via the emission of phonons and photons. Results of three different type of experiments [12-15] have been published testing the idea of the microwave superradiance emission of molecular magnets and we will comment on them.

In the next we will comment on the experiments performed to detect what it is called Quantum Magnetic Deflagration. It has been experimentally elucidated [16, 17] that during an avalanche the magnetization reversal occurs inside a narrow interface that propagates through a crystal at a constant speed of a few meters per second. This process is similar to the propagation of a flame front through a flammable chemical substance and we will describe the experiments we performed using high frequency acoustic waves to control the ignition field of the avalanches and to study the dependence of its velocity on the value of the magnetic field (see Figure 3). These works have opened the door to new way for the study of quantum phenomena in molecular magnets, as well as to study both the magnetic and electric avalanches detected in the phase separated manganites [18] and intermetallic compounds [19].

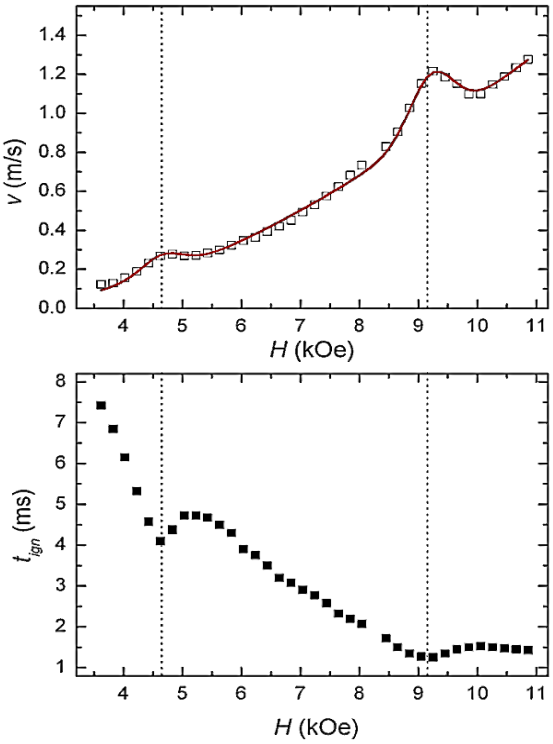

Fig. 3 – Magnetic deflagration speed (up) and ignition time (bottom) as a function of the magnetic field. Vertical lines show the positions of the tunneling resonances

3. QUANTUM DEPINNING OF MAGNETIC VORTEX CORE IN MICRON-SIZE PERMALLOY DISKS

In the absence of applied magnetic field, micron-size disks of soft ferromagnetic materials exhibit the vortex state as the magnetic equilibrium of the system. Its spin field splits into two well differentiated structures: 1) the *vortex core* consisting of a uniform out-of-plane spin component (spatial extension about the exchange length of the material) and 2) the *curling magnetization field* (in-plane spin component), characterized by a non-zero vorticity value. The application of an in-plane magnetic field yields the displacement of the vortex core perpendicularly to the field direction [20]. The vortex shows a special vibrational mode, the *gyrotropic mode*, consisting of the displacement of the vortex core as a whole, following a precessional movement around the vortex centre [21]. Its characteristic frequency belongs to the subGHz range.

We have studied several arrays of permalloy ($Fe_{19}Ni_{81}$) disks with diameter $2R = 1.5$ μm and different thickness ($L = 60$ and 95 nm) under the application of an in-plane magnetic field up to 0.1 T in the range of temperatures 2-300 K. Samples were prepared stacking four 5×5 mm^2 arrays with parallel sides. Measurements were taken in a MPMS magnetometer equipped with the RSO system (sensitivity $5 \cdot 10^{-8}$ emu).

Figure 4 shows the hysteresis loops in the positive range of applied magnetic field at several temperatures for the sample with $L = 95$ nm. From it we observe that the vortex linear regime in the ascending branch should extend from $H = -300$ Oe to 500 Oe (at least). Analogous behaviour has been observed in the other sample with $L = 60$ nm.

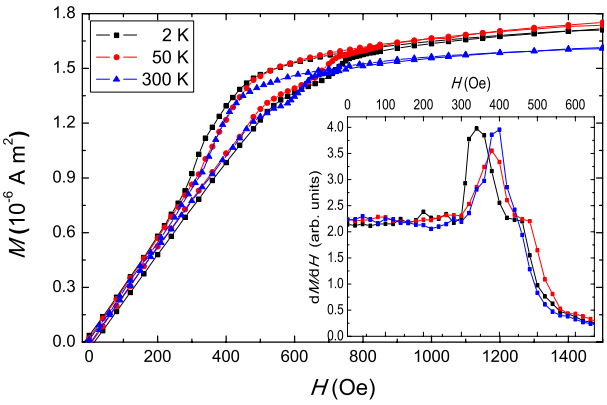

Fig. 4 – $M(H)$ loops at different temperatures (2, 50 and 300 K) for the sample with $L = 95$ nm. The inset shows their numerical derivative dM/dH along the descending branch

Figure 5 shows the ZFC-FC curves measured at an applied magnetic field $H = 300$ Oe (a) and the isothermal magnetic measurements along the descending branch, $M_{des}(H)$, from the Single Domain state ($H = 0.1$ T) to $H = 300$ Oe (b) for the sample with $L = 95$ nm. One could clearly appreciate the onset of magnetic irreversibility below $T = 20$ K. Analogous behaviour has been observed in the other simple.

A simple way to study this magnetic irreversibility is by means of relaxation experiments. Figure 6 shows a set of relaxation measurements of magnetic vortices from the metastable states of the descending branch at $H = 0$ to the equilibrium state (which corresponds to $M = 0$) at several temperatures for the sample with $L = 95$ nm. We observe a logarithmic dependence of the magnetization on the time, which corresponds to a broad distribution of energy barriers. Analogous behaviour has been observed in the other sample.

Figure 7 shows the magnetic viscosity at zero field for both samples. It is obtained computing the slopes

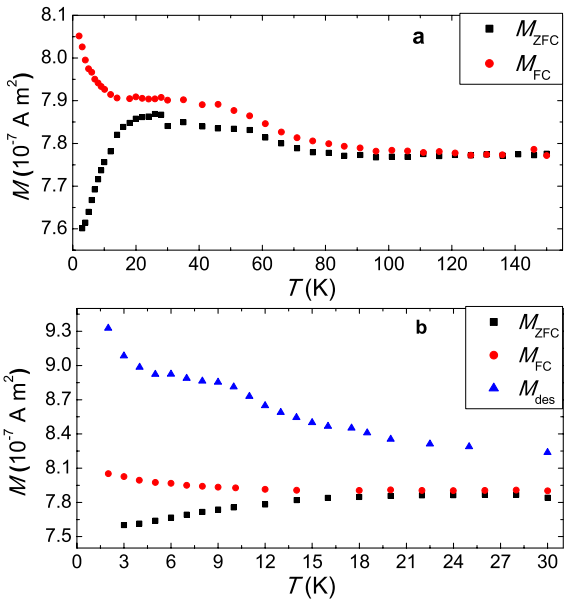

Fig. 5 – ZFC-FC curves at H = 300 Oe (a) and isothermal magnetic measurements along the descending branch at H = 300 Oe for the sample with L = 95 nm

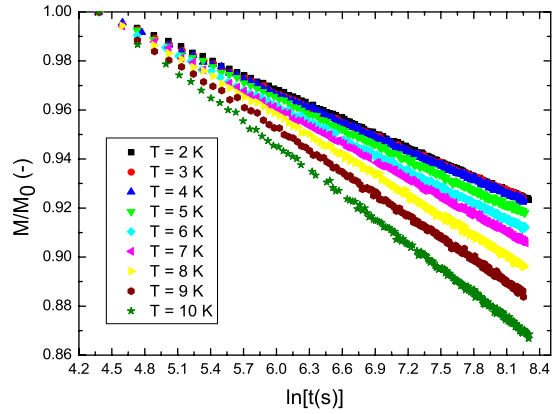

Fig. 6 – Normalized relaxation measurements for the sample with L = 95 nm. M_0 corresponds to the initial point of the relaxation

of the normalized relaxation curves in Fig. 6. Below T = 6 K magnetic viscosity reaches a plateau with a non-zero value, which is an experimental evidence of the quantum tunneling of energy barriers: thermal activation of energy barriers dies out in the limit $T \to 0$. Observation that magnetic viscosity $S(T)$ tends to a finite value different from zero as $T \to 0$ indicates that relaxations are non-thermal in this regime.

The presence of structural defects in the sample can affect the dynamics of the vortex core [22,23]. These structural defects in the disks could be a feasible origin of the energy barriers responsible for the magnetic dynamics of the system. We consider them to be capable of pinning the vortex core, when the applied magnetic is swept, in a non-equilibrium position.

4. QUANTUM TUNNELING IN A TYPE-I SUPERCONDCUTOR

The intermediate state of type-I superconductors has been recently reactivated as an appealing field of

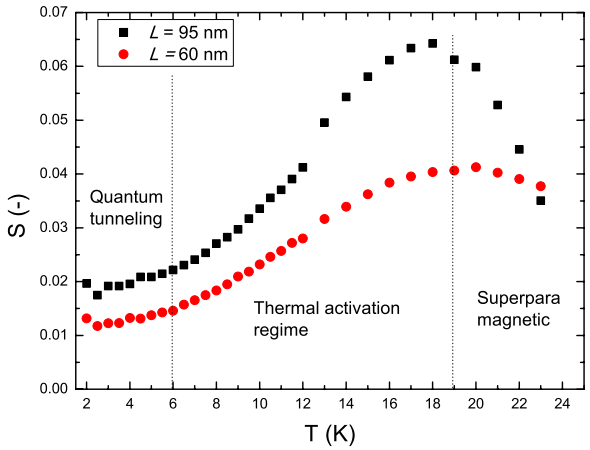

Fig. 7 – Magnetic viscosity S versus temperature T for both samples L = 95 nm (black) and L = 60 nm (red)

experimental and theoretical research one century after the discovery of superconductivity (see Refs [24, 25] for a review). A set of recent works, those by Prozorov and co-workers [26–29] and those by Tejada's group [30–35], have expanded the field of type-I superconductors which was thought to be almost blocked for decades, with the proposal of totally novel phenomena such as the Topological Magnetic Irreversibility (TMI) and the quantum tunneling of Normal-Superconducting Interfaces (NSIs).

The TMI, which is related to the existence of a geometrical energy barrier [26, 27], has been proved to depend on both the shape of the sample and its orientation with respect to the applied magnetic field [27-30]. When the magnetic field is applied along the revolution axis, a defect-free (cylinder)-shaped disk sample exhibits a strong irreversibility between the ascending and descending branches of the hysteresis cycle, which is correlated to the existence of different topologies for the formed flux structures [27]. Normal bubbles embedded in a superconducting phase are observed along the ascending branch of the hysteresis cycle forming the so-called suprafroth state [28], whereas lamellar patterns are observed during flux expulsion. Topological hysteresis in defect-free samples disappears when the magnetic field tends to zero and the system becomes unable to trap any flux line at this field strength [27].

The picture of topological hysteresis strongly changes when pinning defects are present in the sample as physical stress induces defects during the sample preparation in polycrystalls [30]. In such a case, the magnetic irreversibility is enhanced along the descending branch, which depends on the temperature and the nature of the defects, but no appreciable differences were observed along the first magnetization curve (penetration flux curve) of the hysteresis cycle with respect to the defect-free case [33]. Defects affect strongly the capability of the system to trap magnetic flux along the descending (ascending) branch of the hysteresis cycle when the magnetic field is swept back to zero from the normal state. The huge remnant magnetization observed is a strong proof of that [30, 33]. For illustration, Fig. 8 shows isothermal magnetization curves, $M(H)$, taken on a extremelly

pure (99.999 %) Pb disk sample of thickness 0.2 mm and surface area 40 mm^2 with stress defects (see Ref. [32] for sample preparation) when the applied magnetic field is along the revolution axis. The inset shows scaling with $m = M/H_c(T)$ and $h = H/H_c(T)$, where $H_c(T)$ is the so-called thermodinamic critical field (see Ref. [24]). Note that the resulting magnetization curves exhibit all the features described above and the fitting of the data to $H_c(T)$ matches with the well known values of a conventional Pb type-I superconductor.

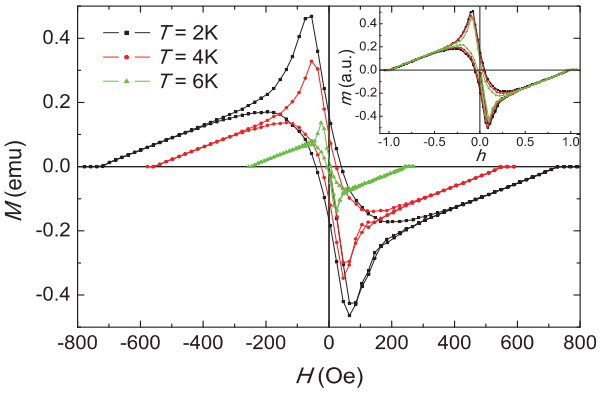

Fig. 8 – Isothermal magnetization curves of a Pb disk when the magnetic field is applied along the revolution axis. The inset shows scaling with $m = M/H_c(T)$ and $h = H/H_c(T)$

Resemblances between the movement of domain walls in ferromagnets and the movement of NSIs in type-I superconductors have led us to interpret the observed enhancement of the hysteresis cycles (with respect to the TMI case. See Fig. 8) as a consequence of the pinning of the interfaces at the defects [32]. In the presence of pinning centers, the interfaces adjust themselves to the pinning potential by developing curvature (bumps or depletions) at the NSI. The effective potential associated with defects during flux expulsion should be then strong enough to effectively pin interfaces along the descending branch for a certain range of magnetic fields and temperatures as the magnetization curves plotted in Fig. 8 indicate. The temperature dependence of the observed hysteresis cycles suggests an inverse field dependence of the pinning potentials [33], being closer to zero when h is closer to the thermodinamical critical field ($h = 1$), and becoming maximum at zero field. As a consequence, when H decreases from the normal state, the onset of irreversibility due to the pinning of interfaces at the defects comes at a temperature and sample dependent critical field, $h^*(T)$, and a suitable landscape for the study of magnetic relaxation processes appears in the system. This magnetic field can be identified either between the ascending and descending branches of the hysteresis cycle or from the difference between the FC magnetic measurements (equilibrium topology for flux expulsion) and the magnetization states followed along the descending branch of the hysteresis cycle.

The dynamics of the pinned NSIs have been tested by performing magnetic relaxation measurements at different states along the descending branch of the hysteresis cycle [34]. The time evolution of the irreversible magnetization proves to be logarithmic for a wide range of temperatures and magnetic field values [32, 35]. This is related to the existence of a broad distribution of energy potentials associated to the defects and it is consistent with the sample preparation procedure. Fitting of the time evolution of the irreversible magnetization to Eq. (3) leads to the determination of the magnetic viscosity of the system, S, at different temperatures T and magnetic field strengths h. Figure 9 shows the resulting temperature dependence of the magnetic viscosity at various h values. Remarkably, it does not extrapolate to zero in the limit of $T \to 0$ in all sets. On the contrary, it tends to a finite temperature-independent value, which depends on the magnetic field strength h. It is an indicative of underbarrier quantum tunneling being the responsible mechanism for the observed magnetic relaxation in this regime [32, 35].

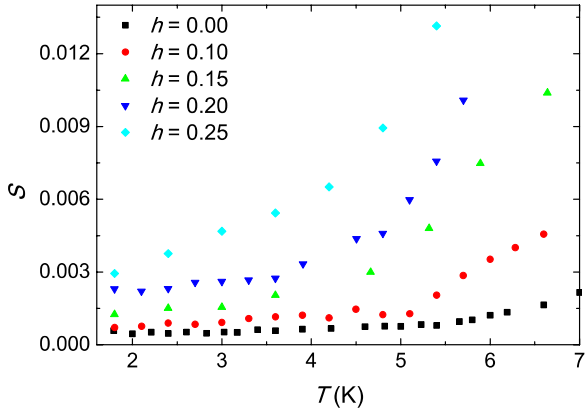

Fig. 9 – Temperature dependence of the magnetic viscosity, $S(T)$, obtained for $h = 0.00$ (squares), $h = 0.10$ (circles), $h = 0.15$ (upward triangles), $h = 0.20$ (downward triangles), and $h = 0.25$ (diamonds)

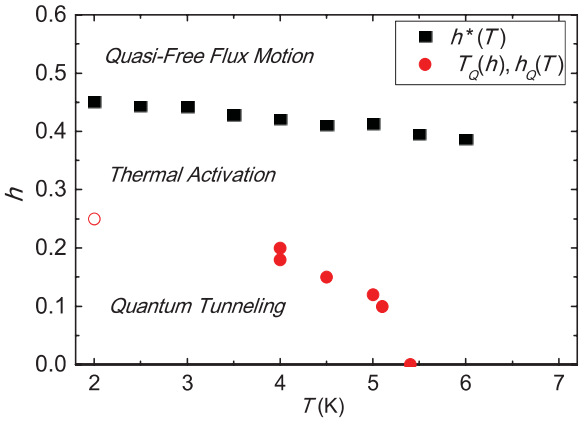

Fig. 10 – Reduced magnetic field vs temperature phase diagram showing the different regimes that describe the dynamics of the NSIs when the initial state lies along the descending branch of the hysteresis cycle. Solid squares correspond to the irreversibility line, $h^*(T)$, that separates the regimes of quasi-free flux motion and thermal activation, while solid circles correspond to the crossover line, $T_Q(h)$ and $h_Q(T)$, that separates the thermal and quantum regimes of magnetic relaxation. The open circle stands for the value of T_Q estimated for $h = 0.25$

From Fig. 9 one can identify a magnetic field-dependent crossover temperature between thermally activated motion and underbarrier quantum transition of the NSIs. In addition, the onset of magnetic irreversibility is identified through the h^* values. Above this value, the regime is called as 'Quasi-Free Flux motion' since defects only play a role in the domain formation but not in the macroscopic properties. According to all this, one can construct the whole phase diagram of the dynamics of NSIs in a type-I superconductor in the presence of defects, see Figure 10. Note that the inverse magnetic field dependence of both magnitudes with h is an indicative of the reduction of the effective potentials associated with defects on h. Recalling the Caldeira-Leggett theory of quantum dissipation, the crossover temperature between quantum and thermal regimes has been formulated in terms of the microscopic parameters of Pb [32]. It has allowed us to identify that bumps formed at the NSI must be of the length of the superconducting coherence length ξ of Pb and that they must move in steps of the nanometric scale (size of the deformation). From the data shown in Fig. 10 one can see that the higher the magnetic field is, the flatter the bumps become. Eventually, they do not form at strong enough applied magnetic field (see Ref [34]). A further complete theory of quantum dissipation of the NSIs in Pb has been developed and fitted well to the experimental data [35].

REFERENCES

1. E. M. Chudnovsky, J. Tejada, *Lectures on Magnetism (with 128 Problems)* (Princeton: Rinton Press: 2006).
2. E. M. Chudnovsky, J. Tejada, *Macroscopic Quantum Tunneling of the Magnetic Moment* (Cambridge: Cambridge University Press: 1998).
3. E. M. Chudnovsky, L. Gunther, *Phys. Rev. Lett.* **60**, 661 (1988).
4. J. Tejada, X. X. Zhang, E. M. Chudnosvky, *Phys. Rev. B* **97**, 14977 (1993).
5. J. Friedman, M. P. Sarachik, J. Tejada, R. Ziolo, *Phys. Rev. Lett.* **76**, 3830 (1996).
6. J. M. Hernandez, X. X. Zhang, F. Luis, J. Bartolomé, J. Tejada, R. Ziolo, *Europhys. Lett.* **35**, 301 (1996).
7. L. Thomas, F. Lionti, R. Ballou, D. Gatteschi, R. Sessoli, B. Barbara, *Nature (London)* **383**, 145 (1996).
8. W. Wernsdorfer, R. Sessoli, *Science* **284**, 133 (1999).
9. S. Hill, J. A. A. J. Perenboom, N. S. Dalal, T. Hathaway, T. Stalcup, J. S. Brooks, *Phys. Rev. Lett.* **80**, 2453 (1998).
10. E. Del Barco, J. M. Hernandez, J. Tejada, N. Biskup, R. Achey, I. Rutel, N. Dalal, J. Brooks, *Phys. Rev. B* **62**, 3018 (2000).
11. M. Dressel, B. Gorshunov, K. Rajagopal, S. Vongtragool, A. A. Mukhin, *Phys. Rev. B* **67**, 060405 (2003).
12. J. Tejada, R. Amigo, J. M. Hernandez, E. M. Chudnovsky, *Phys. Rev. B* **68**, 014431 (2003).
13. A. Hernández-Mínguez, M. Jordi, R. Amigó A. García-Santiago, J. M. Hernández, J. Tejada, *Europhys. Lett.* **69**, 270 (2005).
14. J. Vanacken, S. Stroobants, M. Malfait, V. V. Moshchalkov, M. Jordi, J. Tejada, R. Amigo, E. M. Chudnovsky, D. A. Garanin, *Phys. Rev. B* **70**, 220401 (2004).
15. M. Jordi, A. Hernández-Mínguez, J. M. Hernandez, J. Tejada, S. Stroobants, J. Vanacken, V. V. Moshchalkov, *Europhys. Lett.* **68**, 888 (2004).
16. Y. Suzuki, M. P. Sarachik, E. M. Chudnovsky, S. McHugh, R. Gonzalez-Rubio, N. Avraham, Y. Myasoedov, E. Zeldov, H. Shtrikman, N. E. Chakov, G. Christou, *Phys. Rev. Lett.* **95**, 147201 (2005).
17. A. Hernández-Mínguez, J. M. Hernandez, F. Macià, A. Garcia-Santiago, J. Tejada, P. V. Santos, *Phys. Rev. Lett.* **95**, 217205 (2005).
18. F. Macià, A. Hernández-Mínguez, G. Abril, J. M. Hernandez, A. García-Santiago, J. Tejada, F. Parisi, P. V. Santos, *Phys. Rev. B* **76**, 174424 (2007).
19. S. Velez, J. M. Hernandez, A. Fernandez, F. Macià, C. Magen, P. A. Algarabel, J. Tejada, E. M. Chudnovsky, *Phys. Rev. B* **81**, 064437 (2010).
20. T. Shinjo, T. Okuno, R. Hassdorf, K. Shigeto, T. Ono, *Science* **289**, 930 (2000).
21. S.-B. Choe, Y. Acremann, A. Scholl, A. Bauer, A. Doran, J. Stöhr, A. Padmore, *Science* **304**, 420 (2004).
22. H. Shima, V. Novosad, Y. Otani, K. Fukamichi, N. Kikuchi, O. Kitakamai, Y. Shimada. *J. Appl. Phys.* **92**, 1473 (2002).
23. R. L. Compton, T. Y. Chen, P. A. Crowell, *Phys. Rev. B* **81**, 144412 (2010).
24. For an overview of works performed up to the late 1960s, see *Superconductivity* (Ed. R. D. Parks) (New York: Dekker: 1969), Vol. 2, p. 1235.
25. C. P. Poole Jr, H. A. Farach, R. J. Creswick, R. Prozorov, *Superconductivity, 2nd Edition* (Amsterdam: Accademic Press: 2007), p. 326–333.
26. R. Prozorov, R. W. Giannetta, A. A. Polyanskii, G. K. Perkins, *Phys. Rev. B* **72**, 212508 (2005).
27. R. Prozorov, *Phys. Rev. Lett.* **98**, 257001 (2007).
28. R. Prozorov, A. F. Fidler, J. R. Hoberg, P. C. Canfield, *Nat. Phys.* **4**, 327 (2008).
29. J. R. Hoberg, R. Prozorov, *Phys. Rev. B* **78**, 104511 (2008).
30. S. Vélez, C. Panadès-Guinart, G. Abril, A. García-Santiago, J. M. Hernandez, J. Tejada, *Phys. Rev. B* **78**, 134501 (2008).
31. S. Vélez, A. García-Santiago, J. M. Hernandez, J. Tejada, *Phys. Rev. B* **80**, 144502 (2009).
32. E. M. Chudnovsky, S. Vélez, A. García-Santiago, J. M. Hernandez, J. Tejada, *Phys. Rev. B* **83**, 064507 (2011).
33. S. Vélez, A. García-Santiago, J. M. Hernandez, J. Tejada, e-print arXiv:1105.6218.
34. Saül Vélez, Ricardo Zarzuela, Antoni García-Santiago, Javier Tejada, *Phys. Rev. B* **85**, 064506 (2012).
35. R. Zarzuela, E. M. Chudnovsky, J. Tejada, *Phys. Rev. B* **84**, 184525 (2011).